Theoretical Studies of non Inductive Current Drive by Oscillating Magnetic Fields, Neutral Beams and Helicity Injection in High β Plasmas

R. Farengo, A. F. Lisfchitz, H. E. Ferrari, S. Bouzat
Centro Atómico Bariloche e Instituto Balseiro, 8400 Bariloche, RN, Argentina
E-mail:farengo@cab.cnea.gov.ar

R. A. Clemente
Instituto de Fisica Gleb Wataghin, Universidade Estadual de Campinas, 13083-970 Campinas, SP, Brazil

Recent advances on theoretical studies of various non inductive current drive methods (neutral beam injection, oscillating magnetic fields and helicity injection) which apply to compact toroids and RFPs are presented.

1. Neutral Beam Injection into Field Reversed Configurations Sustained by Rotating Magnetic Fields

The Monte Carlo Code already used to study neutral beam injection (NBI) into high flux field reversed configurations (FRC) [1] was employed to study tangential neutral beam injection (TNBI) into moderate flux FRCs sustained by rotating magnetic fields (RMF) [2]. The main goal of this study was to determine the minimum increases in experimental parameters, and the corresponding optimal beam parameters, necessary for efficient beam coupling. Considering FRCs with the same size as those produced in the Translation, Confinement and Sustainment (TCS) experiment [3], four different equilibria were analyzed. Most of the results presented below were obtained using a somewhat higher magnetic field and temperature than can be obtained in present experiments (B_{ext}=75 mT, $T_{e,i}$=140 eV, n_e=5×10^{19} m^{-3}, r_s=0.3 m, r_c=0.37 m, L_s=2m, χ_s= r_s/r_c=0.8). Two injection geometries, shown in Fig. 1, were considered. In one case the beam was injected through the ends (I), at a small angle (α) to the FRC axis while in the other (II) the beam was injected almost perpendicular, at some point along the separatrix.

The results obtained without including the RMF show that even at the lowest practical energies (10 keV), trapping D beams is very difficult due to the low magnetic flux and high χ_s value, typical of RMF sustained FRCs. Hydrogen beams were therefore employed in all the calculations. In injection through the ends the beam current is concentrated in the mirror region and very low current drive efficiencies and deposited power result. This is seen in Fig. 2, which shows the spatial distribution of the beam current density for a 10 keV, 100 A H beam in a case without RMF.

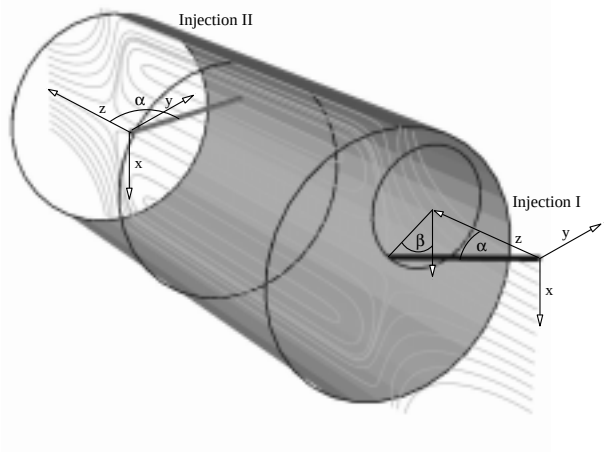

Fig. 1. The two injection geometries employed

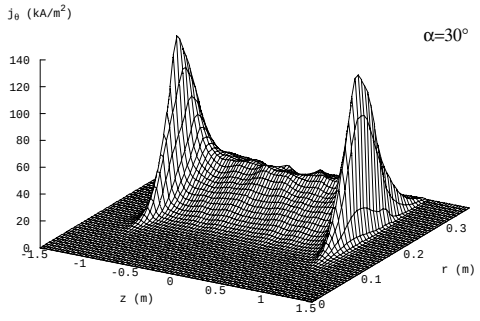

Fig. 2. Spatial distribution of the beam current

Much higher efficiencies are obtained for almost perpendicular injection at some point along the separatrix (II). Fig. 3 shows the current drive efficiency as a function of the impact parameter (b) for a 10 keV H beam injected at the midplane with various injection angles (α). In this case the beam current is distributed almost uniformly along the FRC, as shown in Fig. 4, and similar efficiencies are obtained for injection at different axial positions due to the very racetrack shape of the equilibria employed.

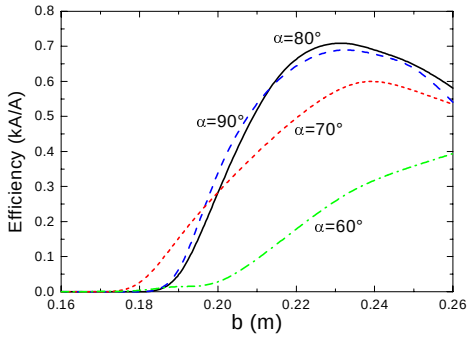

Fig. 3. Efficiency vs. injection angle for a 10 keV H beam injected at the midplane, without RMF

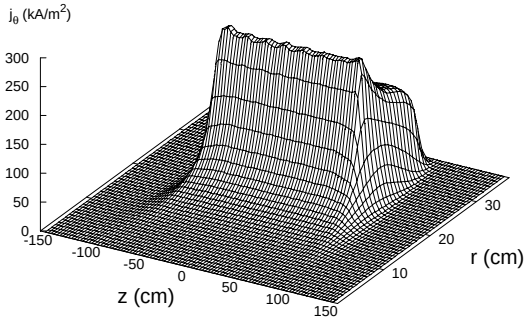

Fig. 4. Spatial distribution of beam current density for injection at z_i=0.75 m with α=90 and b=0.215 m.

When a RMF, characterized by its amplitude (B_ω), frequency (ω) and penetration range (δ) is included the efficiency decreases. Fig 5 shows the efficiency as a function of the RMF amplitude (5a), penetration range (5b) and frequency (5c). At a fixed frequency of 1 Mrad/s the efficiency decreases monotonically with the amplitude and penetration of the RMF. The dependence upon frequency is more complicated and a sharp reduction is seen at $\omega \approx 5$ Mrad/s.

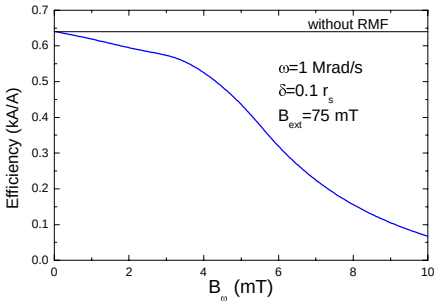

Fig. 5a. Efficiency vs. amplitude of the RMF.

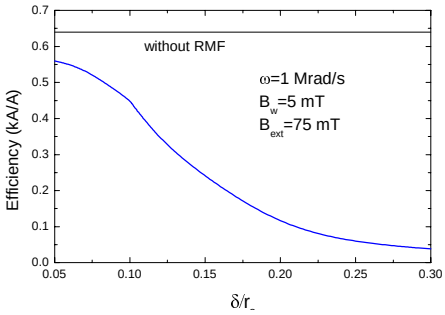

Fig. 5b. Efficiency vs. penetration of the RMF.

The resonance occurs when the frequency of the RMF is close to the frequency of rotation of the beam ions around the FRC axis. Present experiments operate with $\omega \approx 1$ Mrad/s, $\delta/r_s \approx 0.1$ and $B_\omega \approx 5$ mT. With these parameters the resonance will not be a problem and a 100 A beam could provide about one-fourth of the total current. Since the angular momentum deposited by the beam will be of the same order as the RMF deposited torque the simultaneous use of both methods appears very attractive.

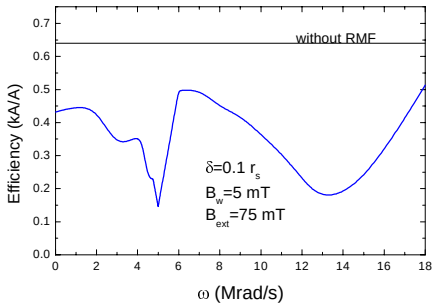

Fig. 5c. Efficiency vs. frequency of the RMF.

2. Current Drive with Oscillating Helical Fields in RFPs

Rotating Manetic Fields (RMF) are effective to sustain the current in FRCs, which have no toroidal field [3]. When both poloidal and toroidal currents are needed a natural extension of the RMF method is the double helix scheme, where two sets of helical coils are employed. Bertram [4] studied numerically the double-helix scheme using a simple plasma model: fixed ions, a linearized Ohm's law for electrons, uniform density and no temperature effects. After examining in detail two representative cases, weakly and strongly resistive plasmas, he concluded that strong toroidal fields do result in drastic reductions in the amount of current that can be driven and consequently the method would not be suitable for large tokamaks. The weakly resistive limit was recently reconsidered in a semi analytic calculation [5] which showed the possibility of efficient current drive for screw and reversed field pinches (RFP). Owing to the limitations of the linearization procedure employed in Refs [4] and [5], where in general only first harmonics are retained, it is of interest to develop a full numerical calculation that properly accounts for the non linear terms in Ohm's law.

Here we use a non-linear Ohm's law to study current drive by a double helix traveling magnetic field. An infinite plasma column of radius a, subject to the action of external magnetic fields varying like $\exp i(\theta + kz - \omega t)$ and a uniform static external longitudinal magnetic field B_0, is considered. The ions are assumed to be fixed and electron inertia, thermal effects and density gradients are neglected. With these approximations Ohm's can be written as:

$$\mathbf{j} = -en\mathbf{u} = \frac{1}{\eta}\left(\mathbf{E} - \frac{\mathbf{j}\times\mathbf{B}}{en}\right) \tag{1}$$

where $\eta = m\nu/e^2 n$ and n, m, $-e$, $\mathbf{u}$ and ν are the electronic density, mass, charge, velocity and collision frequency respectively. The density and collision frequency are assumed to be uniform and the displacement current is neglected in Ampere's law.

Normalizing the radial coordinate and the wave vector with the plasma radius ($x=r/a$, $h=ka$) the analysis is simplified by introducing non-dimensional helical coordinates $x_1=x$, $x_2=\theta+kz$ and x_3 ignorable, with unit vectors $\hat{e}_1=\hat{e}_r$, $\hat{e}_2 = (\hat{e}_\theta + hx\hat{e}_z)/d$ and $\hat{e}_3 = (\hat{e}_z - hx\hat{e}_\theta)/d$, where $d = (1+h^2x^2)^{1/2}$. A generic vector can be expressed as $\mathbf{C}=C_1\,\hat{e}_r + (C_2\,\hat{e}_2 + C_3\,\hat{e}_3)/d$ with $C_2=C_\theta+hxC_z$ and $C_3=C_z-hxC_\theta$ quasi-helical components [5]. In addition, the time, magnetic field, vector potential and current density are normalized as follows:

$$\tau = \omega t, \qquad \boldsymbol{\beta} = \frac{\mathbf{B}}{B_\omega}, \qquad \boldsymbol{\alpha} = \frac{\mathbf{A}}{aB_\omega}, \qquad \mathbf{i} = \mu_0 a\frac{\mathbf{j}}{B_\omega} \tag{2}$$

where B_ω is the amplitude of the traveling magnetic field, in the absence of plasma, at the column center. Using Faraday's law to express the electric field in terms of $\boldsymbol{\alpha}$ Eq.(1) becomes:

$$\mathbf{i} = -2\lambda^2\frac{\partial\boldsymbol{\alpha}}{\partial\tau} - \gamma\,\mathbf{i}\times\boldsymbol{\beta}, \qquad \text{where} \quad \lambda^2 = \frac{a^2\mu_0\,\omega}{2\eta}, \quad \gamma = \frac{B_\omega}{en\eta} \tag{3}$$

From Eq. (3) we obtain two coupled equations for the evolution of the third quasi-components of $\boldsymbol{\alpha}$ and $\boldsymbol{\beta}$ (since only α_3 and β_3 appear we omit the sub-index 3 from now on):

$$\frac{\partial\alpha}{\partial\tau} = \frac{1}{2\lambda^2}\left(\Delta^{\otimes}\alpha + \frac{2h}{1+h^2x^2}\beta\right) + \frac{\gamma}{2\lambda^2}\frac{1}{x}\left(\frac{\partial\beta}{\partial x_2}\frac{\partial\alpha}{\partial x} - \frac{\partial\beta}{\partial x}\frac{\partial\alpha}{\partial x_2}\right) \tag{4}$$

$$\frac{\partial\beta}{\partial\tau}=\frac{1}{2\lambda^2}\left(\Delta^{\otimes}\beta-\frac{2h}{1+h^2x^2}\left(\Delta^{\otimes}\alpha+\frac{2h\beta}{1+h^2x^2}\right)\right)-\frac{\gamma}{2\lambda^2}\frac{1}{x}\left[\frac{2h^2x}{1+h^2x^2}\left(\frac{\partial\beta}{\partial x_2}\beta-\Delta^{\otimes}\alpha\frac{\partial\alpha}{\partial x_2}\right)+\frac{\partial\alpha}{\partial x}\frac{\partial\Delta^{\otimes}\alpha}{\partial x_2}-\frac{\partial\alpha}{\partial x_2}\frac{\partial\Delta^{\otimes}\alpha}{\partial x}+\frac{4h}{1+h^2x^2}\left(\frac{\partial\beta}{\partial x_2}\frac{\partial\alpha}{\partial x}-\frac{\partial\beta}{\partial x}\frac{\partial\alpha}{\partial x_2}\right)\right]$$

where (5)

$$\Delta^{\otimes}\equiv\frac{\partial^2}{\partial x^2}+\frac{1-h^2x^2}{1+h^2x^2}\frac{1}{x}\frac{\partial}{\partial x}+\frac{1+h^2x^2}{x^2}\frac{\partial^2}{\partial x_2^2}\,.$$

Eqs. (4) and (5) were solved with a 2D (x, x_2) finite differences code with a fourth order Runge-Kutta scheme for the time integration. It was assumed that the current density vanishes outside the plasma and the external coils are located sufficiently far from the column in order to use simple analytical expressions for their contribution. The coil current was switched on smoothly in less than one period. The code was checked by recovering the steady state results obtained by Bertram in the very resistive limit ($\lambda=4$ and $\gamma=3.55$).

With the model of Refs. [4] and [5], it is not possible to show good penetration when the ratio γ/λ^2 (which measures the efficiency of the scheme in terms of applied oscillating field and maximum amount of diamagnetism or paramagnetism of the longitudinal magnetic field) is less than unity. We are using the non-linear code to better assess the actual limits of the method in terms of γ/λ^2. So far we have been able to explore the efficiency up to values of γ=20 and λ=12 which corresponds to $\gamma/\lambda^2\cong 0.14$ (smaller than in the very resistive limit examined by Bertram) finding good penetration and efficiency when the scheme is applied to RFPs or screw pinches (always when diamagnetism is produced).

We show, in Fig. 6 a plot of the azimuthal ($I_\theta=\int_0^1 dx<i_\theta>$) and axial ($I_z=2\pi\int_0^1 dx\,x<i_z>$) currents as a function of time for γ=20, λ =12, h=1 and B_0=1. It is clear that after a transient phase a steady state with significant currents is reached. Since changing h it is possible to obtain different ratios of I_z/I_θ this method could also be used in conjunction with other current drive methods to obtain the desired current profiles.

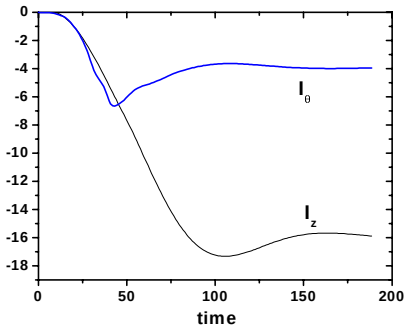

Fig. 6. Current vs time for λ=12 and γ=20

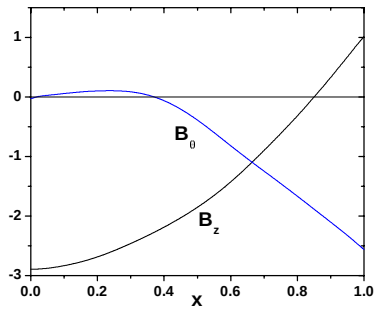

Fig. 7. Magnetic field profiles for λ=12 and γ=20

Fig. 7 shows the steady state radial profiles of B_θ and B_z for the same parameters as in Fig. 6. The parabolic shape of the B_z profile indicates that the oscillating fields have deeply penetrated into the plasma and the electrons rotate almost rigidly, with frequency ω, in the azimuthal direction. Work is in progress to better reproduce the experimental profiles and run the code at higher values of λ and γ.

3. Current Drive with two Rotating Magnetic Fields in FRCs

When a single RMF is employed to sustain the current in FCRs, ion spin-up due to electron-ion collisions reduces the current [6]. Clemente [7] proposed using two magnetic fields rotating in opposite senses. Using a two fluid model with finite electron inertia and no viscosity he showed the existence of steady-state solutions where both species rotate as rigid rotors and the torques deposited on electrons and ions, averaged over the azimuthal angle and the period of the oscillating fields, are equal and opposite and balance the torque due to electron-ion collisions.

To further investigate this scheme we calculated analytically the time dependent torques deposited on both species using the same assumptions as in Ref. [7]. The following dimensionless parameters are introduced (variables and parameters not defined in this section have the same meaning as those defined in Sec. 2):

$$c_1 = \frac{\nu}{\omega}, \qquad c_2 = \frac{eB_\omega}{m_e\omega}, \qquad c_3 = \frac{a^2\mu_0 n_0 e^2}{m_e}, \qquad S_e^{\pm} = \omega_e \pm 1, \qquad S_i^{\pm} = \frac{m_i}{m_e}\left(-\omega_i \pm 1\right)$$

where ω_e and ω_i are the rotation frequencies of electrons and ions. The angular and time dependence is expanded as: $Q(x,\theta,\tau) = (Q^-(x)e^{i(\theta-\tau)} + Q^+(x)e^{i(\theta+\tau)}) + c.c.$. The two RMFs, are introduced by specifying the z component of the vector potential far from the plasma:

$$\alpha_z(x_c,\theta,\tau) = x_c\,(e^{i(\theta-\tau)} + a^+ e^{i(\theta+\tau)}) + c.c. \tag{6}$$

where a^+ is the ratio of the amplitudes of the two RMFs and x_c>>1. When S_i^+ << 1 and S_e^- << 1, the torque on the electrons can be written as the sum of a constant part plus a time dependent term:

$$\langle\mu_e\rangle \approx \langle\langle\mu_e\rangle\rangle + \frac{1}{2}c_2c_3\left(1+\frac{m_e}{m_i}\right)\mathrm{Im}\left\{\left(-1+S_i^+/S_e^+ - i\left(S_e^- + {S_i^+}^2/S_e^+\right)/c_1\right)a^+|x|^2e^{2i\tau}\right\} \tag{7}$$

where, $\langle\mu_e\rangle = 1/(2\pi)\int_0^{2\pi} d\theta\,\mu_e$ and $\langle\langle\mu_e\rangle\rangle \approx \frac{1}{2}c_2c_3(1+m_e/m_i)\left[S_e^-|x|^2\right]$ is the value calculated in Ref. [7]. A similar expression is obtained for the ions. When $a^+\approx 1$ the oscillatory term can be larger than the constant part.

To study the effect of viscosity and the oscillations in the torque and we developed a time dependent, two fluid code with finite electron mass. Neglecting u_r, and introducing dimensionless variables we obtained the following set of equations:

$$\frac{\partial u_{e,i_z}}{\partial\tau} = -\frac{c_2}{c_3}\frac{\langle u_{e,i_\theta}\rangle}{x}\frac{\partial u_{e,i_z}}{\partial\theta} + c_3p_{e,i}\frac{\partial\alpha_z}{\partial\tau} + c_2p_{e,i}\frac{\langle u_{e,i_\theta}\rangle}{x}\frac{\partial\alpha_z}{\partial\theta} - c_1p_{e,i}\left(u_{e,i_z} - u_{e,i_z}\right) + \bar{\eta}_{e,i}\Delta u_{e,i_z}$$

$$\frac{\langle\partial u_{e,i_\theta}\rangle}{\partial\tau} = c_3p_{e,i}\left\langle\frac{\partial\alpha_\theta}{\partial\tau}\right\rangle + c_2p_{e,i}\left\langle\frac{u_{e,i_z}}{x}\frac{\partial\alpha_z}{\partial\theta}\right\rangle - c_1p_{e,i}\left(\langle u_{e,i_\theta}\rangle - \langle u_{e,i_\theta}\rangle\right) + \bar{\eta}_{e,i}\Delta_x\langle u_{e,i_\theta}\rangle \tag{8}$$

$$\nabla^2\mathbf{A} = \mathbf{u}_e - \mathbf{u}_i$$

where,

$$\mathbf{u} = \frac{\mu_0 e n_0 a}{B_\omega}\mathbf{v}, \quad \bar{\eta}_e = \frac{0.73}{0.96}\sqrt{\frac{m_i}{m_e}}\bar{\eta}_i, \quad \bar{\eta}_i = \frac{\eta_i}{n_0m_ia^2\omega}, \quad \Delta_x = \frac{\partial^2}{\partial x^2} + \frac{1}{x}\frac{\partial}{\partial x} - \frac{1}{x^2}, \quad p_e = 1, \quad p_i = -\frac{m_e}{m_i}$$

We note that if we leave c_1, c_2 and c_3 fixed and change m_e/m_i what we are actually doing is to change the ion mass. At x=1 we require that the viscous stresses vanish and the external axial magnetic field be consistent with the assumed plasma current. The axial component of the vector potential is specified at x=x_c as indicated in Eq. (6). The initial condition considered

has electrons and ions rigidly rotating in opposite senses. We do not investigate here how this state can be reached. One possibility would be to use a single magnetic field to accelerate the electrons and neutral beams for the ions.

We show, in Fig. 8 the radial profile of the azimuthal electron velocity at different times for c_1=1, c_2 =100, c_3=2, m_i/m_e=100, $\overline{\eta_i}$ =0.01 and a^+=1 (equal amplitude of both fields). The initial rigid rotation disappears because the torque on the electrons has large oscillations (see Eq. (7)) and neither field is able to entrain them. In Fig. 9 we shown the azimuthal ion velocity at x=0.95 for different values of a^+ and the same parameters as in Fig. 8. When a^+=0 there is only one rotating field and the ions accelerate due to collisions with the electrons. For a^+ = 0.1 the torque on the ions is not enough to compensate the collisions with the electrons and they accelerate as in the case with a^+=0. When a^+ =0.3 a stationary state is reached with both species rotating in opposite senses.

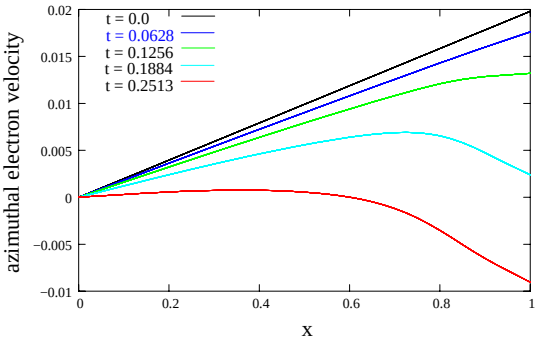

Fig. 8. Radial profile of <$u_{e\theta}$>

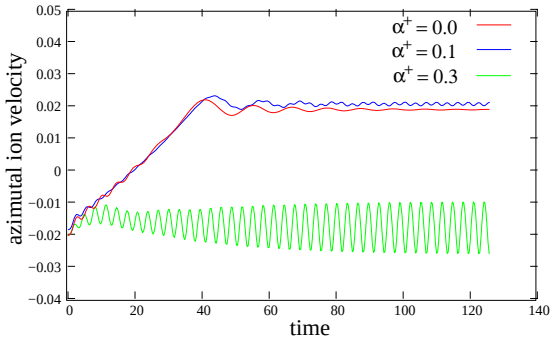

Fig 9. Time evolution of <$u_{i\theta}$>at x=0.95

In Fig. 10 we show the azimuthal ion velocity as a function of time for different values of the viscosity, a^+=0.3 and the other parameters as in Fig.8. It is clear that the viscosity value is critical. If it is too small ($\overline{\eta_i}$ =0.001), the oscillations in the torque destroy the synchronism. If it is too high ($\overline{\eta_i}$ =0.1) u_z is too small and the torque is not enough to compensate the collisions. Preliminary results obtained with larger mass ratios show that the method can work for realistic values of m_i/m_e. In Fig. 11 we show a case with a^+=0.3, m_i/m_e=1000 and c_1=10, c_2=1000, c_3=20 and $\overline{\eta_i}$ =0.0075 where a steady-state is also reached. In summary, we have shown that reducing the amplitude of one of the RMF it is possible to maintain stationary solutions with ions and electrons rotating in opposite senses.

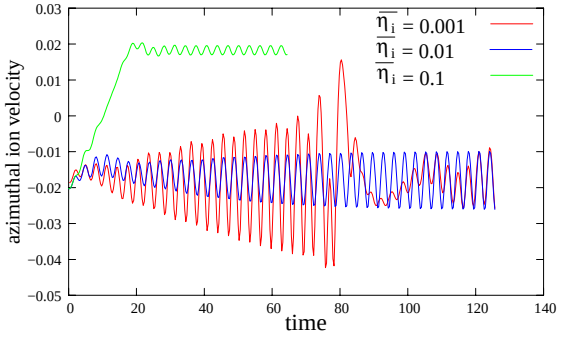

Fig. 10. Time evolution of <$u_{i\theta}$>at x=0.95

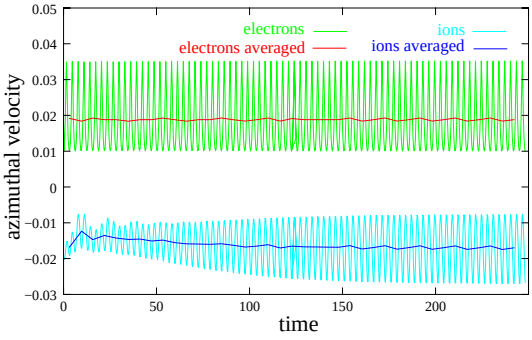

Fig. 11. Time evolution of <$u_{i\theta}$>and <$u_{e\theta}$>at x=0.95

4. Minimum Dissipation States in Plasmas Sustained by Helicity Injection

Analytical solutions for the minimum dissipation states of a flux core spheromak sustained by helicity injection through magnetized electrodes are presented. The configuration considered is shown in Fig. 12. The flux conserver is covered on the inside with a dielectric and voltages

$\pm V/2$ are applied to the electrodes. Helicity balance ($\dot{K}_{inj} = \dot{K}_{dis}$) [8], $\nabla\cdot$B=0 and Ampere's law are the constraints employed in the minimization. We Introduce the following functional,

$$W = \int \eta\, \mathbf{j}^2\, d^3r - \frac{\lambda}{\mu_0}\left[\int \eta\, \mathbf{j}\cdot\mathbf{B}\, d^3r + \int_{electrodes} \Phi\ \mathbf{B}\cdot d\mathbf{S}\right] - \int \gamma\, \nabla\cdot\mathbf{B}\, d^3r + \int \mathbf{C}\cdot\left(\mu_0\mathbf{j} - \nabla\times\mathbf{B}\right) d^3r \qquad (9)$$

where η is the plasma resistivity (assumed uniform), λ, γ and **C** are Lagrange multipliers and Φ is the voltage applied on the electrodes. Setting the first variation of W equal to zero we obtain the following Euler-Lagrange equation for the current density [9]:

$$\nabla\times\mathbf{j} - \lambda\,\mathbf{j} + \frac{\mu_0}{2\eta}\nabla\gamma = 0 \qquad (10)$$

From $\nabla\cdot\mathbf{j}$=0 we obtain $\nabla^2\gamma$=0. The *natural* boundary conditions, obtained by requesting that the surface term in δW vanish, are $j_\theta=(\lambda/2)B_\theta$ on the entire vessel and $\gamma=\lambda\Phi/\mu_0$ on the electrodes. In addition, we request that the normal components of **j** and **B** vanish at $r=a$.

In the equation for γ, Φ should be set equal to the potential at the electrodes, $\Phi(\pm L) = \mp V/2$. However, in defining the potential at the electrodes, we face a delicate problem due to the limitations of the MHD model to describe the potential fall occurring near an electrode. The details of the problem will be discussed elsewhere. Here we only mention that it is necessary to consider a different value $V_0<V$ of the potential in order to obtain realistic values for the external current I_z. We will show later how V_0 can be determined from the desired value of I_z. A possible option to improve the model is to consider a very high resistivity next to the electrodes but this complicates considerably the analytic treatment.

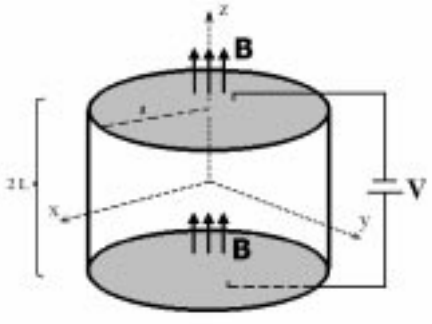

Fig. 12. Configuration considered

In what follows we employ dimensionless variables: $r/a \to r$, $\lambda/a \to \lambda$, $\mathbf{B}/B_{ext} \to \mathbf{B}$, $\mathbf{j}\mu_0 a/B_{ext} \to \mathbf{j}$, $\mu_0 a\gamma/(\eta_0 B_{ext}) \to \gamma$, $\eta/\eta_0 \to \eta$, $V\mu_0/B_{ext}\eta_0 \to V$, $L/a \to L$, where B_{ext} is the magnitude of the external field and η_0 a typical resistivity value in Ωm. The general solution of Eq. (10) for **j** and **B** can be written as:

$$\mathbf{j} = \xi + \mu_l\nabla\gamma \qquad \mathbf{B} = \xi/\lambda + \mu_l\nabla\times\left(\tilde{\gamma}\hat{z} + f(r)\,\hat{z}\right) + \nabla\chi \qquad (11)$$

where $\mu_l=\mu_0/2\eta\lambda$ and:

$$\xi = \nabla\times(\psi\,\hat{z}) + \frac{1}{\lambda}\nabla\times\nabla\times(\psi\,\hat{z}), \quad \nabla^2\chi = 0 \qquad \nabla^2\psi + \lambda^2\psi = 0$$

The functions $\tilde{\gamma}$ and $f(r)$ are defined as [10]: $\tilde{\gamma} = \int_{-L}^{z}\gamma(r,z')\,dz'$, $\quad f(r) = -\int_0^r dr_2\,\frac{1}{r_2}\int_0^{r_2} r_1\,\gamma_z(r_1,-L)\,dr_1$

where $\gamma_z=\partial_z\gamma$. The problem is then reduced to finding the solutions for χ, γ and ψ. Note that χ contributes to the magnetic field with the irrotational term $\nabla\chi$ which represents the external magnetic field. The boundary conditions employed are: $B_r(1,z)=0$, $j_r(1,z)=0$, $j_\theta(1,z)=(\lambda/2)B_\theta$, $\nabla\chi(r,\pm L)\cdot\mathbf{n}=1$, $\gamma(r,\pm L)=\mp\lambda V_0/2$ and $j_\theta(r,\pm L)=(\lambda/2)B_\theta(r,\pm L)$. The solution with azimuthal symmetry can be written as:

$$\psi = A_0\, J_0(\lambda r) + \sum 2\,A_i\,\cosh(k_i z)\,J_0(k_i' r), \qquad \gamma = C_0\, z, \qquad \chi = z \qquad (12)$$

where k_i' is the ith positive zero of J_0 and $k_i'^2 = \lambda^2 + k_i^2$. The constants A_i and C_0 can be written in terms of the system parameters.

Calculating the total current through the electrodes it is possible to show that due to the natural boundary conditions employed $V_0=I_z \eta L/\pi$. With this equation we determine the value of V_0 given I_z, η and L. The value of λ is determined from the helicity balance condition, where the actual value of the potential at the electrodes is employed. For given values of the external parameters two spheromak-type solutions, with different values of λ exist. The one with the lowest value (λ_1) has the open flux on the inside while in the one with the largest value (λ_2) has the flux wrapped around the spheromak [8].

The parameters employed in the calculation are similar to those proposed for the Proto-SPHERA experiment [11], a=0.33 m, L=1.3 a, B_{ext}=0.1 T, $I_z=6\times10^4$ A and V=50 V. In Fig. 13 we show λ_1, λ_2 and the total toroidal current for both solutions as functions of η. Fig. 14 shows flux contours for both solutions with $\eta=10^{-5}$. We have also calculated non axisymmetric (m=1) solutions which do not contribute to I_z and the total flux through the electrodes. These solutions have $\mathbf{j}_1(1,z).\mathbf{n}=0$, $\mathbf{B}_1(1,z).\mathbf{n}=0$ and are given by [9]:

$$\psi_1 = J_1(qr)\cos(q'z+\theta), \quad \gamma_1 = -s\,I_1(qr)\sin(qz+\theta), \quad \chi_1 = 0 \tag{13}$$

where q and s are determined by the boundary conditions at r=1 and $q'^2=\lambda^2-q^2$. Preliminary calculations show lower dissipation rates with the mixed state in the parameter regime corresponding to spheromak formation. This could indicate that the non axisymmetric state, which is needed to sustain the spheromak, is the preferred one in driven scenarios.

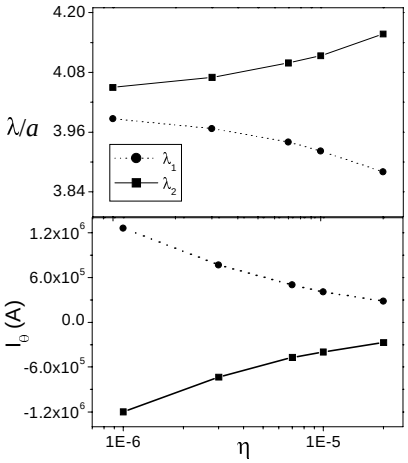

Fig. 13. λ and toroidal current vs. resistivity

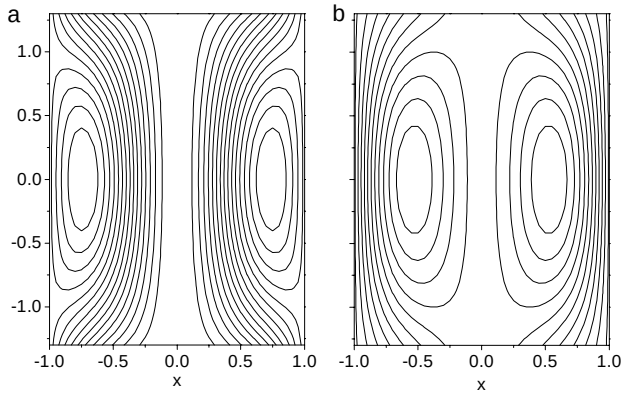

Fig. 14 Flux contours for both type of solutions

Acknowledgements

Work partially supported by *Agencia Nacional de Promoción Científica y Tecnológica* of Argentina. RAC thanks partial support from *Conselho Nacional de Desenvolvimento Científico e Tecnológico* of Brazil. The contribution of A. Hoffman to Sec. 1 is acknowledged.

[1] LIFSCHITZ A. F. et al. Nucl. Fusion **42**, 863 (2002).
[2] LIFSCHITZ A. F. et al. Nucl. Fusion **44**, 1015 (2004).
[3] HOFFMAN A. L. et al. Fusion Techn. **41**, 92 (2002).
[4] BERTRAM W. K. Plasma Phys. Contr. Fusion **30**, 425 (1988).
[5] CLEMENTE R. A. and FARENGO R. (2003) Braz, J, Phys. **33, 867.**
[6] LIFSCHITZ A. F. et al. Plasma Phys. Contr. Fusion **45**, 999 (2003).
[7] CLEMENTE R. A. J. Phys. Soc. Japan **67**, 3450 (1998).
[8] FARENGO R. and CAPUTI K. Plasma Phys. Contr. Fusion **44**, 1707 (2002).
[9] WANG C. Y. and BHATTACHARJEE A. Phys. Fluids B, **12**, 3462 (1991).
[10] MORSE P. and FESHBACH H. *Methods of Theoretical Physics*, McGraw Hill, 1953.
[11] ALLADIO F. et al. Proto-SPHERA proposal, www.frascati.enea.it/ProtoSphera. (2000).